Integrating Tensile Parameters in Mass-Spring System for Deformable Object Simulation

Vincent Baudet, Michael Beuve, Fabrice Jaillet, B. Shariat, Florence Zara

Integrating Tensile Parameters in Mass-Spring System for Deformable Object Simulation

Vincent Baudet, Michael Beuve, Fabrice Jaillet, Behzad Shariat, and Florence Zara

Abstract—Besides finite element method, mass-spring system is widely used in Computer Graphics. It is indubitably the simplest and most intuitive deformable model that takes into account elastic considerations. This discrete model allows to perform with ease interactive deformations as well as to handle complex interactions. Thus, it is perfectly adapted to generate visually plausible animations. However, a drawback of this simple formulation is the relative difficulty to control efficiently realistic physically-based behaviors. Indeed, none of the existing models has succeeded in dealing with this satisfyingly. Moreover, we demonstrate that the mostly cited technique in the literature, proposed by Van Gelder, is far to be exact in most real cases, and consequently, this model can not be used in simulation. So, we propose a new general 3D formulation that reconstructs the geometrical model as an assembly of elementary hexahedral "bricks". Each brick (or element) is then transformed into a mass-spring system. Edges are replaced by springs that connect masses representing the vertices. The key point of our approach is the determination of the stiffness springs to reproduce the correct mechanical properties (Young's modulus and Poisson's ratio) of the reconstructed object. We validate our methodology by performing some numerical experiments. Finally, we evaluate the accuracy of our approach, by comparing our results with the deformation obtained by finite element method.

Index Terms—Discrete Modeling, Physical Simulation, Mass-Spring System, Rheological Parameters.

1 Introduction

Finite elements methods (FEM) are generally used to accurately simulate the behavior of 3D deformable objects. They require a rigorous description of the boundary conditions so that the amplitudes of the applied strains and stresses must be well defined in advance to choose either a small - with Cauchy's description - or a large deformation context - with St Venant Kirchoff's description for example. Indeed, the accuracy of each context is optimized within its deformation domain.

Mass-spring systems (MSS) have largely been used in animation because of their simple implementation and their possible applications for a large panel of deformations. They consist in describing a surface or a volume with a mesh in which the global mass is uniformly distributed over the mesh nodes. The tensile behavior of the object is simulated by the action of springs, connecting the mesh nodes. Then, Newton's laws govern the dynamics of the model, and the system composed of Ordinary Differential Equations (ODEs) can be solved via numerical integration over time. In computer graphics, MSS-based animations are generally proposed to deal with interactive applications and to allow unpredictable interactions. They are adapted to virtual reality environments where many unpredicted collisions may occur and where objects can undergo deformations and/or mesh topology changes. Medical or surgery simulators present another example of their possible applications. Nevertheless these models generally fail to represent accurately the behavior of real deformable objects (characterized by their Young's modulus and Poisson's ratio) because of the difficulty to obtain correct springs stiffness constant.

In this paper, our aim is not to compare MSS and FEM models, but to propose a new solution to enhance MSS, making them more compatible with the requirements of physical realism, by giving a solution to obtain the springs stiffness constants according to elastic parameters. Section 2 presents a state of the art of mass-spring systems and particularly their parameterization. Moreover, in this section, we present published solutions allowing the determination of springs constant to obtain a realistic behavior of the simulated object. Section 3 describes Van Gelder's model, which incorporates spring parameters calculated from the elasticity parameters. We prove that this model cannot simulate correctly 2D deformations and in section 4, we present our alternative approach to calculate springs stiffness constants according to tensile parameters of the simulated object. In section 5, we present how we simulate an object composed of our model. Then, section 6 presents some experimental results. Finally, some concluding remarks and perspectives are given in section 7.

2 Related Work

Mass-spring systems have been used to model textiles [11], [14], [23], long animals such as snakes, or soft organic tissues, like muscles, face or abdomen, where the cutting of tissue can be simulated [16], [17], [19], [20]. Moreover, these systems have been used to describe a wide range of different elastic behaviors such as

• *Université de Lyon, CNRS, Université Lyon 1, LIRIS, SAARA team, UMR5205, F-69622, France*

Septembre 2009.

anisotropy [3], heterogeneity [24], non linearity [4] and also incompressibility [22].

However, where FEMs are built upon elastic theory, mass-spring models are generally far from being accurate. Indeed, in these models, springs stiffness constants are usually empirically set and consequently, it is difficult to reproduce the true behavior of a given material with these models. Thus, if the MSS have allowed convincing animations for visualization purposes, their drawbacks refrain the generalization of their use when greater resolution is required, like for mechanical or medical simulators. For more details, an extensive review can be found in [18].

Consequently, the graphics community has proposed solutions based on simulated annealing algorithms [9], [13] to estimate springs stiffness constants to correctly mimic material properties. Usually, these solutions consist in applying random values to different springs constants and comparing the obtained model behavior with some mechanical experiments in which results are either analytically well known or can be numerically obtained. Then, the springs stiffness constants that induce the greatest error are corrected to minimize the discrepancies. More recently, Bianchi *et al.* [2] proposed a similar approach based on genetic algorithms using reference deformations simulated with finite element methods. However, the efficiency of these approaches depends on the number of springs and is based on numerous mechanical tests leading to a quite expensive computation. Moreover, the process should be repeated after any mesh alteration and the lack of reference solution is an obstacle to the generalization of the method to other cases.

Instead of a trial-and-error process, a formal solution that parameterizes the springs should save computer resources. In this context, two approaches were explored. The Mass-Tensor approach [6], [21] aims at simplifying finite element method theory by a discretization of the constitutive equations on each element. Despite of its interest, this approach requires pre-computations and the storage of an extensive amount of information for each mesh component (vertex, edge, face, element).

The second approach has been proposed by Van Gelder [25] and has been referenced in [3], [5], [7], [15], [20], [26]. In this approach, Van Gelder proposes a new formulation for triangular meshes, allowing the calculation of springs stiffness constant according to elastic parameters of the object to simulate (Young's modulus E, and Poisson's ratio ν). This approach combines the advantages of an accurate mechanical parameterization with a hyper-elastic model, enabling either small or large deformations. However, in next section, we show that numerical simulations completed by a Lagrangian analysis exhibit the incompatibility of the proposal with the physical reality. Indeed, the Van Gelder's approach is restricted to $\nu = 0$.

An extension of Van Gelder's method has been recently presented in [12] for tetrahedra, hexahedra and some other common shapes, but still remains limited to $\nu = 0,3$ that prevents their use when accurate material properties are required.

Finally, Delingette [8] proposed a formal connection between springs parameters and continuum mechanics for the membranes. He succeeded to simulate realistically the membrane behavior for the specific case of Poisson's ratio $\nu = 0,3$ with regular MSS. The extension of this approach to 3D is not yet available.

3 Van Gelder Model

In 1998, Van Gelder [25] proposed a formulation for 2D triangular mass-spring systems, allowing to calculate springs stiffness constants according to elastic parameters of the object to simulate. In this model (see Fig. 1), the stiffness constant of a spring, with rest length c, representing the common edge of two neighboring triangles of the mesh (T_i) of surfaces $|T_i|$ and with edges c, a_i, b_i (with $i \in \{1, 2\}$) is given by

$$k_c = \sum_{i=1}^{n} \frac{E}{1+\nu} \frac{|T_i|}{c^2} + \frac{E\,\nu}{1-\nu^2} \frac{a_i^2 + b_i^2 - c^2}{8\,|T_i|}, \qquad (1)$$

with ν, the Poisson's ratio and E, the corresponding 2D Young's modulus of the simulated material. Note that, afterward, these coefficients will be noted E_{VG} and ν_{VG} (coefficients initially used in the Van Gelder (VG) system to obtain the stiffness constants).

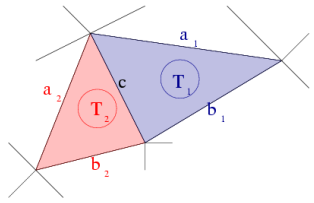

Fig. 1. Notations used for Van Gelder's model.

Moreover, Van Gelder's published experimentations are restricted to $\nu = 0$ to avoid negative value of k_c. But, to cope with majority of elastic materials, we used Van Gelder's approach to simulate materials with $\nu \geq 0$. In particular, we reproduced the well-known tensile test using a bar of dimensions $l_0 \times h_0$ (see Fig. 2 (Left)). Thus, the bar, fixed at its base, is elongated by a force $\vec{F}_{tensile}$, generating a stretch η and a compression of 2δ at equilibrium.

For our test, the bar is meshed by four symmetrical Van Gelder triangles and the springs stiffness constants were calculated according to equation (1). This configuration implies the same stiffness constant for the four diagonal springs (k_d), and equal stiffness constants for springs laying on two parallel edges (k_{l_0} and k_{h_0}) (see Fig. 2 (Right)).

According to Hooke's law, and for such boundary conditions, the theoretical Young's modulus E and Poisson's ratio ν are defined by:

$$E = \frac{F_{tensile}/l_0}{\eta/h_0}, \quad \nu = \frac{2\delta/l_0}{\eta/h_0}. \qquad (2)$$

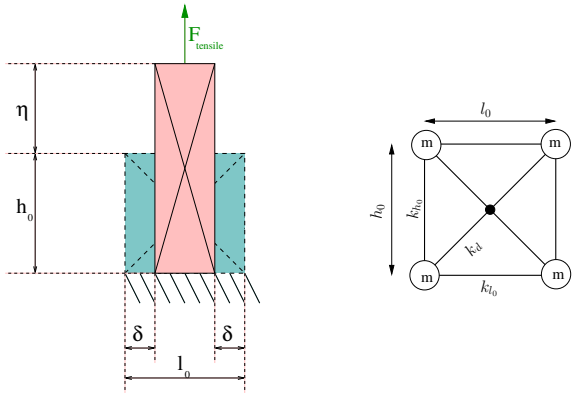

Fig. 2. (Left) Tensile test bar. (Right) 2D rectangular element meshed by 4 VG triangles involving several springs with stiffness constants k_{l_0}, k_{h_0} and k_d.

Thus, if we note E and ν the Young's modulus and Poisson's ratio computed after the simulation according to the obtained deformations, checking whether the relations $\nu_{VG} = \nu$ and $E_{VG} = E$ are satisfied, will certify that VG's model follows Hooke's law. However, the simulations results presented in Table 1 show that this is not the case. Even when Poisson's ratio is set to zero, we note a 25% error on the Young's modulus value, although the authors claimed that their model was valid for this specific value, used for simulating membranes.

Poisson's ratio		Young's modulus (Pa.m)	
ν_{VG}	ν	E_{VG}	E
0.0	0.5	0	0
		1	0.75
		100	75.00
		1000	750.00
0.25	0.57	0	0
		1	0.63
		100	62.86
		1000	628.57
0.5	0.66	0	0
		1	0.56
		100	55.56
		1000	555.56

TABLE 1
Comparison tests between input parameters (ν_{VG}, E_{VG}) and theoretical values (ν, E) obtained after deformation.

To complete this observation, we propose a demonstration within the Lagrangian formulation framework. Thereby we had to:

1) Define springs potential energy according to their elongations (η and δ) and potential energy of applied forces,
2) Define the Lagrangian as the sum of the different static potential energies (note that kinetic energies are null),
3) Deduce the values of the deformations (η and δ) by applying Least Action Principle,
4) Calculate the actual value of the Young's modulus and the Poisson's ratio of the bar.

Thus, we have first to define the springs potential energy according to the elongation. Using equation (1), we find stiffness constants for the three different kinds of springs:

$$\begin{aligned} k_{l_0} &= \frac{1}{4}\left[\frac{h_0 E_{VG}}{l_0(1+\nu_{VG})} + \frac{E_{VG}\,\nu_{VG}({h_0}^2 - {l_0}^2)}{(1-{\nu_{VG}}^2) l_0 h_0}\right], \\ k_{h_0} &= \frac{1}{4}\frac{({h_0}^2\nu_{VG} - {l_0}^2)E_{VG}}{(-1+{\nu_{VG}}^2)\, l_0 h_0}, \\ k_d &= \frac{2E_{VG}\, l_0 h_0}{(1+\nu_{VG})\left({l_0}^2+{h_0}^2\right)} + \frac{E_{VG}\,\nu_{VG}\,\left({l_0}^2+{h_0}^2\right)}{2\,(1-{\nu_{VG}}^2)\, l_0 h_0}. \end{aligned}$$

Then, for small deformations, the potential energy associated to these stiffness constants is defined by $E_{p_i} = \frac{1}{2}\, k_i\, d_i^2$, with $i \in \{l_0, h_0, d\}$ and d_i the corresponding deformations equal to 2δ for k_{l_0}, η for k_{h_0} and $\frac{1}{2}\sqrt{{l_0}^2 - 4l_0\delta + 4\delta^2 + {h_0}^2 + 2h_0\eta + \eta^2} - \frac{1}{2}\sqrt{{l_0}^2+{h_0}^2}$ for k_d. So, we obtain:

$$\begin{aligned} E_{p_{l_0}} &= \frac{1}{2}\left[\frac{h_0\, E_{VG}}{l_0(1+\nu_{VG})} + \frac{E_{VG}\,\nu_{VG}\,({h_0}^2 - {l_0}^2)}{(1-{\nu_{VG}}^2) l_0 h_0}\right]\delta^2, \\ E_{p_{h_0}} &= \frac{1}{8}\frac{({h_0}^2\nu_{VG} - {l_0}^2)E_{VG}}{(-1+{\nu_{VG}}^2) l_0 h_0}\,\eta^2, \\ E_{p_d} &= -\frac{A\, B\, E_{VG}}{16\, h_0 l_0\,(-1+{\nu_{VG}}^2)\left({l_0}^2+{h_0}^2\right)^2} + O\left(\eta^2, \delta^2\right), \end{aligned}$$

with

$$\begin{aligned} A &= \left({h_0}^2\eta^2 - 4\, l_0 h_0 \delta\, \eta + 4\, {l_0}^2\delta^2\right), \\ B &= \left(-2\, {l_0}^2 {h_0}^2 \nu_{VG} + {l_0}^4\nu_{VG} + {h_0}^4\nu_{VG} + 4\, {l_0}^2 {h_0}^2\right). \end{aligned}$$

Consequently for small deformations, the Lagrangian associated to this tensile test, involving 2 springs of stiffness constant k_{l_0}, 2 springs of stiffness constant k_{h_0} and 4 springs of stiffness constant k_d, is defined by:

$$L = F_{tensile}\eta - 2E_{p_{l_0}} - 2E_{p_{h_0}} - 4E_{p_d}.$$

Then, we apply Least Action Principle to obtain the values of the deformations (η and δ) leading to solve:

$$\frac{\partial L}{\partial \eta} = 0, \quad \frac{\partial L}{\partial \delta} = 0.$$

We obtain

$$\begin{aligned} \eta &= -2\,\frac{F_{tensile}\, h_0\, C}{E_{VG}\, l_0\, D}, \\ \delta &= \frac{(1+\nu_{VG})\, F_{tensile}\, H}{I\, E_{VG}}, \end{aligned}$$

with

$$C = 4\,{l_0}^4{\nu_{VG}}^2 - {l_0}^4\nu_{VG} - 2\,{l_0}^2{h_0}^2\nu_{VG} - {h_0}^4\nu_{VG} - 5\,{l_0}^4 - 2\,{l_0}^2{h_0}^2 - {h_0}^4$$

$$D = {l_0}^4\nu_{VG} - 6\,{l_0}^2{h_0}^2\nu_{VG} + {h_0}^4\nu_{VG} + 5\,{l_0}^4 + 2\,{l_0}^2{h_0}^2 + 5\,{h_0}^4$$

$$H = -2\,{l_0}^2{h_0}^2\nu_{VG} + {l_0}^4\nu_{VG} + {h_0}^4\nu_{VG} + 4\,{l_0}^2{h_0}^2$$

$$I = {l_0}^4\nu_{VG} - 6\,{l_0}^2{h_0}^2\nu_{VG} + {h_0}^4\nu_{VG} + 5\,{l_0}^4 + 2\,{l_0}^2{h_0}^2 + 5\,{h_0}^4$$

Consequently, according to these deformations, the Young's modulus of the bar after deformation is defined by

$$E = \frac{F_{tensile}/l_0}{\eta/h_0} = -\frac{1}{2}\frac{I\, E_{VG}}{C}$$

and the Poisson's ratio by

$$\nu = \frac{2\delta/l_0}{\eta/h_0} = -\frac{H}{4\,{l_0}^4{\nu_{VG}}^2 - 5\,{l_0}^4 - 2\,{l_0}^2{h_0}^2 - {h_0}^4}.$$

Thus, for a bar of dimension $l_0 \times h_0 = 1 \times 1$, we obtain:

$$E = \frac{1}{2}\frac{E_{VG}(\nu_{VG}-3)}{\nu_{VG}^2 - \nu_{VG} - 2},\ \nu = \frac{1}{2-\nu_{VG}}.$$

Consequently, the relations $E = E_{VG}$ and $\nu = \nu_{VG}$ are even not satisfied. Moreover, we notice that the Young's modulus depends on the Poisson's ratio, although the two characteristics should be totally independent in linear, isotropic and homogeneous materials [10]. Thereby, this model can hardly be used to realistically control the elastic parameters.

4 A NEW PARAMETERIZATION APPROACH

Our approach is based on hexahedral mesh, as currently and widely used within the FEM framework. To better demonstrate the basis of our solution, we begin with the parameterization of a 2D rectangular mass-spring systems (MSS). Indeed, as in FEM, any complex object can be obtained by assembling of these 2D elements [1]. Then, we will extend our solution to 3D elements.

4.1 Case of a 2D element

Let us consider a given 2D rectangular element with rest dimensions $l_0 \times h_0$. This element is composed of four edge springs and two diagonal ones to integrate the role of the Poisson's ratio. The same stiffness constant (k_{h_0} or k_{l_0}) is set on two parallel edges, and (k_d) is identically set for the two diagonal stiffness springs.

In addition to the behavior related to Young's modulus and Poisson's ratio, the model should be able to correctly undergo a shearing stress according to a defined shear modulus G. In 2D, this quantity is measured by applying two opposed forces F_{shear} involving a shear stress F_{shear}/l_0 on two opposite edges of the rectangular element. The material response to the shearing stress is a lateral deviation of angle θ and a displacement η (see Fig. 3).

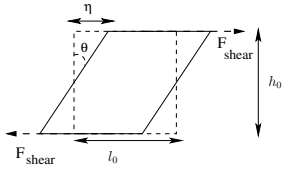

Fig. 3. Experimentation to measure 2D shear modulus: a rectangular element is subject to 2 opposed forces, generating a deviation angle θ and a displacement η.

Though, the shear modulus is defined as:

$$G = \frac{tan\,(\theta) \times F_{shear}}{l_0} = \frac{F_{shear}\ h_0}{l_0\ \eta} \simeq \frac{\theta \times F_{shear}}{l_0} \text{ when } \theta \to 0.$$

For linear elastic, isotropic and homogeneous materials, this coefficient is linked to Young's modulus and Poisson's ratio by $E = 2\,G\,(1+\nu)$.

To determinate the spring coefficients that permit to correctly simulate these mechanical experiments, we follow the next four steps [1]:

1) For each experiment, define the Lagrangian equation (sum of potential energies).
2) Apply Least Action Principle to get Newton's equations.
3) Apply the measured mechanical characteristics definition to build a set of equations linking spring coefficients to mechanical characteristics.
4) Finally, solve the whole system.

Thus, our process begins with the determination of the Lagrangian equation for each experiment, and more precisely we start by the shearing experiment. Indeed, in this experiment only diagonal springs are stressed. Consequently, the Lagrangian equation defining this characteristic depends only on k_d, the stiffness constant of diagonal springs. This means that diagonal springs are totally correlated to shear modulus and that their stiffness can be calculated independently of the two others spring coefficients.

So, the deformation of each diagonal springs is defined by:

$$\begin{aligned}\delta_d &= \sqrt{(l_0 \pm \eta)^2 + h_0^2} - \sqrt{l_0^2 + h_0^2},\\ &\sim \frac{\pm\,\eta\,l_0}{\sqrt{l_0^2+h_0^2}} + O(\eta^2).\end{aligned}$$

Thus, the Lagrangian equation for shearing, involving 2 springs of stiffness k_d, is defined by:

$$\begin{aligned}L &= F_{shear}\eta - 2E_{p_d}\\ &= F_{shear}\eta - 2\times\frac{1}{2}k_d{\delta_d}^2\\ &= F_{shear}\eta - k_d\frac{\eta^2\ l_0^2}{l_0^2+h_0^2}.\end{aligned}$$

Then the minimization of the energy is done for:

$$\frac{\partial L}{\partial \eta} = 0 = F_{shear} - k_d\frac{2\,\eta\,l_0^2}{l_0^2+h_0^2}.$$

It reads:

$$\eta = \frac{F_{shear}(l_0^2+h_0^2)}{2\,l_0^2\,k_d}.$$

Finally, using the shearing definition and linking to E and ν for isotropic and homogeneous materials, we obtain the following relation:

$$k_d = \frac{E\,(l_0^2+h_0^2)}{4\,l_0\,h_0\,(1+\nu)}. \quad (3)$$

Note that for a square mesh element we obtain:

$$k_d = \frac{E}{2\,(1+\nu)} = G.$$

Then, we continue the parameterization to find stiffness constants of the others springs (k_{l_0} and k_{h_0}), by doing two elongation experimentations in lateral and longitudinal direction. We obtain two equations from each elongation experiment, 4 in total [1]. This over-constrained system admits one solution for $\nu = 0.3$, as stated by Lloyd *et al.* [12] and Delingette [8]. But, this result is not satisfactory because we wish to simulate the behavior of any real material. Consequently, we have to add two degrees of freedom to solve this problem.

We note that the Poisson's ratio defines the thinning at a given elongation, *i. e.* it determines the orthogonal forces to the elongation direction. Thus, we introduce for each direction a new variable that represents this orthogonal force. We will note $F_{\perp h_0}$ and $F_{\perp l_0}$ the orthogonal force to h_0 and l_0, respectively. For example, Fig. 4 presents the corrective forces added to the system for an elongation stress $\sigma = F_{tensile}/h_0$. We can observe that a corrective force is generated for each mass of the system.

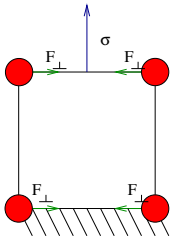

Fig. 4. Corrective forces added to the initial 2D system according to an elongation stress $\sigma = F_{tensile}/h_0$.

Thus, the addition of these 2 new variables leads to a system of 4 equations with 4 unknowns. Note that this kind of correction is equivalent to the *reciprocity principle* used in FEM [10]. Thus, for a constraint F_{h_0} according to h_0, we obtain the following Lagrangian equation (involving 2 springs of constant stiffness k_{l_0}, 2 springs of constant stiffness k_{h_0} and 2 springs of constant stiffness k_d):

$$\begin{aligned} L &= F_{h_0}\eta - 4F_{\perp h_0}\,2\delta - 2E_{p_{l_0}} - 2E_{p_{h_0}} - 2E_{p_d} \\ &= F_{h_0}\eta - 4F_{\perp h_0}\,2\delta - 4\,k_{l_0}\delta^2 - k_{h_0}\eta^2 - k_d {d_d}^2 \end{aligned}$$

with

$$\begin{aligned} d_d &= \sqrt{(h_0+\eta)^2 + (l_0 - 2\delta)^2} - \sqrt{l_0^2 + h_0^2} \\ &\sim \frac{h_0\,\eta - 2\,l_0\,\delta}{\sqrt{h_0^2 + l_0^2}} + O(\eta^2, \delta^2) \end{aligned}$$

the deformation of the diagonal springs. Then, using the definition obtained for k_d in the equation (3), we solve $\frac{\partial L}{\partial \eta} = 0$ and $\frac{\partial L}{\partial \delta} = 0$, and we obtain:

$$\eta = \frac{1}{2}\frac{l_0(4k_{l_0}h_0F_{h_0}\nu - 4EF_{\perp h_0}h_0 + 4k_{l_0}h_0F_{h_0} + El_0F_{h_0})}{4k_{h_0}l_0k_{l_0}h_0\nu + 4k_{h_0}l_0k_{l_0}h_0 + Eh_0{}^2k_{l_0} + k_{h_0}l_0{}^2E},$$

$$\delta = \frac{1}{4}\frac{h_0(-16k_{h_0}l_0F_{\perp h_0} - 16k_{h_0}l_0\nu F_{\perp h_0} - 4EF_{h_0}h_0 + El_0F_{h_0})}{4k_{h_0}l_0k_{l_0}h_0\nu + 4k_{h_0}l_0k_{l_0}h_0 + Eh_0{}^2k_{l_0} + k_{h_0}l_0{}^2E}.$$

Then, using the definitions of Young's modulus and Poisson's ratio, we obtain k_{l_0} and k_{h_0}, but this time according to this new potential $F_{\perp h_0}$. Then, by imposing the symmetry of k_{l_0} with k_{h_0} (*i. e.* by imposing the achievement of the same Young's modulus and Poisson's ratio for an elongation test and its orthogonal), we can restrain the corrective forces and thus obtain the separate formulations of k_{l_0}, k_{h_0} and $F_{\perp h_0}$. Thus, the solution of the system is (with $(i,j) \in \{l_0, h_0\}^2$ and $i \neq j$):

$$k_i = \frac{E\left(j^2\,(3\,\nu + 2) - i^2\right)}{4\,l_0\,h_0\,(1+\nu)}, \quad F_{\perp i} = \frac{i\,F_i\,(1-3\nu)}{8j}. \tag{4}$$

Note that the experimentation according to l_0 would permit to obtain the same stiffness constants and formulations for the corrective forces.

To sum up, each element of our 2D mass-spring system is defined by six springs with three different stiffness constants (k_{l_0}, k_{h_0}, k_d) and by two elongation/compression corrective forces $(F_{\perp l_0}, F_{\perp h_0})$. These coefficients and corrective forces are defined by equations (3) and (4) which integrate Young's modulus and Poisson's ratio of the simulated deformable object.

4.2 Generalisation to 3D elements

Our 3D model is the generalization of our 2D approach by the use of parallelepiped elements. Let's consider a 3D element of our system with dimensions $x_0 \times y_0 \times z_0$.

4.2.1 *Geometry of our 3D model*

As in 2D, to ensure homogeneous behavior, springs laying on parallel edges need to have the same stiffness constant. Thus, we have to determine only 3 stiffness coefficients for these edges: k_{x_0}, k_{y_0} and k_{z_0}. In addition, some diagonal springs are necessary to reproduce the thinning induced by the elongation. Fig.5 displays three possible configurations for these diagonal links:

- M1: diagonal springs located on all faces,
- M2: only inner diagonals,
- M3: combination of both inner and face diagonals.

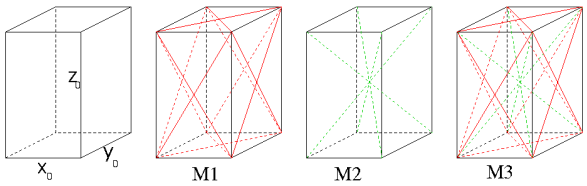

Fig. 5. Three possible configurations for integrating diagonal connections in the 3D element composition.

Prior to the above configuration choice, let's present our springs parameterization approach. As in 2D, we propose a methodology within the Lagrangian framework, according to the following procedure. For each experiment that determinates an elastic characteristic:

1) We build the Lagrangian as the sum of the springs potential due to elongation as well as the potential of external forces, since kinetic term is null.

2) We establish a second order Taylor's expansion of the Lagrangian in deformations and apply *least action principle*.
3) We obtain a set of equations using the mechanical characteristics as input parameters, and we solve this system to get stiffness coefficients.

To solve the system, the number of unknowns has to be equal to the equations number (constraints). Three equations result from each elongation experiment (one for the Young's modulus and one for the Poisson's ratio along each direction orthogonal to the elongation). Thus, we obtain 9 equations for the three elongation directions for all possible configurations. For shearing equations, we have 6 equations for configurations M1 and M3 (2 equations for each shearing plane), and 3 equations for configuration M2 (1 equation for each shearing plane).

For the number of unknowns, three degrees of freedom (k_{x_0}, k_{y_0}, k_{z_0}) stem from the parallel edge for all the possible configurations. Then, for the configuration M1, we have two diagonals on each face of the element, *i. e.* 12 diagonals in total. But, by symmetry we have the same stiffness constant for two diagonal springs in a same face, and the same stiffness constants for springs on parallel faces. So, we get only 3 different diagonals stiffness constants for this configuration M1. For configuration M2, we have only 4 inner diagonals with the same stiffness constant. And, as configuration M3 is the combination of the two priors configuration, we have to determine 4 stiffness constants

Table 2 summarizes these numbers of equations and unknowns. We observe that all geometrical configurations bring to an over-constrained system.

	M1	**M2**	**M3**
Nb of equations for elongation	9	9	9
Nb of equations for shearing	6	3	6
Total number of equations	**15**	**12**	**15**
Nb of unknowns for shearing	3	1	4
Nb of unknowns for elongation	3+(3)	3+(1)	3+(4)
Total number of unknowns	**6**	**4**	**7**

TABLE 2
Number of equations and unknowns according to the chosen geometry.

Nevertheless, configuration M2 is less constrained than the others. Thus, we choose this configuration which corresponds to the model with only inner diagonals modeled by 4 springs with the same stiffness constant noted k_d.

But, before starting our parameterization process to find the four stiffness constants (k_{x_0}, k_{y_0}, k_{z_0} and k_d) of a 3D element in configuration M2, we want to demonstrate that there is no general solution and that the springs on diagonal faces are not mandatory.

4.2.2 Nonexistence of a 3D general solution

For the demonstration of the nonexistence of a 3D general solution, we choose the configuration noted M3, *i.e.* with inner diagonals and face diagonals. Moreover, for notation simplicity, we choose to restrict our 3D element to a cube, *i.e.* where non-diagonal edges are identical. We note x_0 the rest length of these non-diagonal edges and k_{x_0} the stiffness constant of the corresponding springs. This stiffness coefficient has to satisfy two relations (E and ν). We will see that there is only one solution for $\nu = 0.25$, that is not satisfying for a cube (and by extension for any parallelepiped).

Diagonal edges of a 3D face have a length $d_{face} = \sqrt{2}x_0$ and inner diagonal edges have a length $d_{cube} = \sqrt{3}x_0$. We note $k_{d_{face}}$ the stiffness constant of the springs modeling the diagonal edges of a face and $k_{d_{cube}}$ the stiffness constant of the springs modeling the 3D inner diagonal edges.

By symmetry in the cube, the 6 shearing experiments are equivalent and can be resumed into a single equation. If we consider a shearing stress due to a sliding η, we obtain the deformation of the 4 inner diagonals of the cube, and the deformation of the 4 diagonals of the 2 lateral faces of the deformation. We respectively note these deformations $\delta_{d_{cube}}$ and $\delta_{d_{face}}$ with:

$$\delta_{d_{cube}} = \sqrt{(x_0+\eta)^2 + 2x_0^2} - \sqrt{3}\, x_0 \sim \tfrac{\sqrt{3}}{3}\eta + O(\eta^2)$$
$$\delta_{d_{face}} = \sqrt{(x_0+\eta)^2 + {x_0}^2} - \sqrt{2}\, x_0 \sim \tfrac{\sqrt{2}}{2}\eta + O(\eta^2)$$

Thus, the Lagrangian equation for this shearing experiment involving 4 inner diagonals and 4 face diagonals is defined by:

$$\begin{aligned} L &= F_{shear}\eta - 4E_{p_{d_{cube}}} - 4E_{p_{d_{face}}} \\ &= F_{shear}\eta - 4 \times \frac{1}{2}\, k_{d_{cube}}\, {\delta^2}_{d_{cube}} - 4 \times \frac{1}{2}\, k_{d_{face}}\, {\delta^2}_{d_{face}} \\ &= F_{shear}\eta - \frac{2}{3}\, k_{d_{cube}}\eta^2 - k_{d_{face}}\eta^2 \end{aligned}$$

After resolution of the energy minimization and the use of the shearing definition and its link with E and ν, we obtain the following equation:

$$\frac{4\, k_{d_{cube}} + 6\, k_{d_{face}}}{3\, x_0} = \frac{E}{2\,(1+\nu)} = G. \qquad (5)$$

Then, we can incorporate the compressibility experiment. For this, we apply a uniform pressure to the cube, which generates a uniform distortion η. This deformation generates an identical deformation of the inner diagonals and the faces diagonal, defined by:

$$\delta_{d_{cube}} = \sqrt{3\,(x_0+\eta)^2} - \sqrt{3}\, x_0 \sim \sqrt{3}\, \eta + O(\eta^2)$$
$$\delta_{d_{face}} = \sqrt{2\,(x_0+\eta)^2} - \sqrt{2}\, x_0 \sim \sqrt{2}\, \eta + O(\eta^2)$$

The uniform pressure applied to the faces of the cube generates the same surface force noted F_{face}. Thus, the Lagrangian equation of the compressibility experiment, involving 12 side edges, 4 inner diagonals and 12 face diagonals, is defined by:

$$L = 6\ F_{face}\ \frac{\eta}{2} - 12E_{p_{x_0}} - 12E_{p_{d_{face}}} - 4E_{p_{d_{cube}}}$$

$$= 6\ F_{face}\ \frac{\eta}{2} - \frac{12}{2}\ k_{x_0}\ \eta^2 - \frac{12}{2}\ k_{d_{face}}\ {\delta^2}_{d_{face}} - \frac{4}{2}\ k_{d_{cube}}\ {\delta^2}_{d_{cube}}$$

$$= 6\ F_{face}\ \frac{\eta}{2} - 6\ k_{x_0}\eta^2 - 12\ k_{d_{face}}\ \eta^2 - 6\ k_{d_{cube}}\ \eta^2$$

Then, we remember that the compressibility coefficient or Bulk modulus is defined by

$$K = \frac{\Delta P}{\Delta V/V_0}$$

with P the pressure and $\Delta V/V_0$ the volume variation. Moreover, for small deformations, we have the following relation with E and ν:

$$K = \frac{E}{3\,(1-2\nu)}.$$

Consequently, in our experiment the Bulk modulus is defined by:

$$\begin{aligned} K &= \frac{F_{face}/\left(x_0+\eta\right)^2}{\left(\left(x_0+\eta\right)^3 - {x_0}^3\right)/{x_0}^3} \sim \frac{F_{face}}{3\ x_0\eta} + O(\eta^2) \\ &= \frac{E}{3\,(1-2\nu)} \end{aligned}$$

Hence, after resolution of the energy minimization and the use of the definition of the compressibility coefficient with its link with E and ν, we obtain the following equation:

$$\frac{4\ k_{x_0} + 8\ k_{d_{face}} + 4\ k_{d_{cube}}}{3\ x_0} = \frac{E}{3\,(1-2\nu)}. \qquad (6)$$

We can now integrate the laws governing a tensile stress η to take into account Young's modulus and Poisson's ratio. By symmetry, the other directions are compressed of the same value 2δ. Thus, in this experiment, two faces (noted $face_2$) are constricted by keeping their square shape, while the 4 others faces (noted $face_1$), parallel to the elongation, are stretched. Then, diagonal edges are deformed in the following way:

$$\begin{aligned} \delta_{d_{cube}} &= \sqrt{\left(x_0+\eta\right)^2 + 2\left(x_0-2\delta\right)^2} - \sqrt{3}\ x_0 \\ &\sim \frac{\sqrt{3}}{3}\eta - \frac{4\sqrt{3}}{3}\delta + O(\eta^2,\delta^2) \\ \delta_{d_{face_1}} &= \sqrt{\left(x_0+\eta\right)^2 + \left(x_0-2\delta\right)^2} - \sqrt{2}\ x_0 \\ &\sim \frac{\sqrt{2}}{2}\eta - \sqrt{2}\delta + O(\eta^2,\delta^2) \\ \delta_{d_{face_2}} &= \sqrt{2\left(x_0-2\delta\right)^2} - \sqrt{2}\ x_0 \\ &\sim -2\sqrt{2}\delta + O(\delta^2) \end{aligned}$$

Then, the Lagrangian associated to this tensile experiment, involving 4 elongated side edges, 8 compressed side edges, 4 diagonals of constricted faces ($face_2$), 8 diagonals of stretched faces ($face_1$) and 4 inner diagonals, is defined by:

$$\begin{aligned} L &= F_{tensile}\eta - \frac{4}{2}k_{x_0}\eta^2 - \frac{8}{2}k_{x_0}(2\delta)^2 - \frac{4}{2}k_{d_{face}}(-2\sqrt{2}\delta)^2 \\ &\quad - \frac{8}{2}k_{d_{face}}\left(\frac{\sqrt{2}}{2}\eta - \sqrt{2}\delta\right)^2 - \frac{4}{2}k_{d_{cube}}\left(\frac{\sqrt{3}}{3}\eta - \frac{4\sqrt{3}}{3}\delta\right)^2 \\ L &= F_{tensile}\eta - 2k_{x_0}\eta^2 - 16k_{x_0}\delta^2 - 16k_{d_{face}}\delta^2 \\ &\quad - 4k_{d_{face}}\left(\frac{\sqrt{2}}{2}\eta - \sqrt{2}\delta\right)^2 - 2k_{d_{cube}}\left(\frac{\sqrt{3}}{3}\eta - \frac{4\sqrt{3}}{3}\delta\right)^2 \end{aligned}$$

After resolution of the energy minimization and the use of Young's modulus and Poisson's ratio definitions, we obtain the following equations:

$$E = \frac{12k_{d_{cube}}k_{d_{face}} + 24k_{d_{face}}^2 + 24k_{x_0}^2 + 60k_{x_0}k_{d_{face}} + 24k_{x_0}k_{d_{cube}}}{x\left(6k_{x_0} + 9k_{d_{face}} + 4k_{d_{cube}}\right)}$$

$$\nu = \frac{2k_{d_{cube}} + 3k_{d_{face}}}{6k_{x_0} + 9k_{d_{face}} + 4k_{d_{cube}}} \qquad (7)$$

Consequently, we have to resolve a system of equations (5), (6) and (7). One solution can be found for the Poisson's ratio value $\nu = 0.25$ but this is not a versatile solution. So, we have demonstrated that there is no general solution in 3D for a cube, and by extension for any parallelepipedic shape.

4.2.3 Parameterization

Now, we can start our parameterization process with configuration M2 to find the four stiffness constants (k_{x_0}, k_{y_0}, k_{z_0} and k_d) of a 3D element of our mass-spring model.

Shearing experiment

Note that, for small shearing ($\theta \approx 0$), only diagonal springs are stressed. Thus, as in 2D, the Lagrangian equation defining this characteristic depends only on the stiffness constant k_d of the different diagonals. This means that, as in 2D, the diagonal springs fully define the shearing modulus; and their stiffness constant k_d can be determined independently of the other stiffness coefficients. Thus, like in 2D, we begin the parameterization with the shearing experiment.

Let apply a shearing in the (x_0, y_0) plane along x_0 direction. In this experiment, two diagonals are stretched while the two others are compressed. The deformation of each diagonal is defined by:

$$\begin{aligned} \delta_d &= \sqrt{\left(x_0 \pm \eta\right)^2 + y_0^2 + z_0^2} - \sqrt{x_0^2 + y_0^2 + z_0^2}, \\ &\sim \frac{\pm\, x_0\ \eta}{\sqrt{x_0^2 + y_0^2 + z_0^2}} + O(\eta^2). \end{aligned}$$

Thus, the Lagrangian equation for this shearing experiment involving the 4 diagonal springs of stiffness

constant k_d is defined by:

$$\begin{aligned} L &= F_{shear}\eta - 4E_{p_d} \\ &= F_{shear}\eta - 4 \times \frac{1}{2} k_d \ {\delta_d}^2 \\ &= F_{shear}\eta - k_d \frac{2\ \eta^2\ x_0^2}{x_0^2 + y_0^2 + z_0^2} \end{aligned}$$

Then, after the solving of the energy minimization and the use of the shearing definition and its link with E and ν, we obtain:

$$k_d = \frac{E\ z_0\left(x_0^2 + y_0^2 + z_0^2\right)}{8\ (1+\nu)\ x_0\ y_0}.$$

But, if we do again this shearing experiment for the two others directions, we will obtain two others values for the stiffness constant k_d and at the end, we will obtain:

$$k_{d_i} = \frac{E\ i\ \sum_{j\in\{x_0,y_0,z_0\}} j^2}{8(1+\nu)\Pi_{\{l\in\{x_0,y_0,z_0\},l\neq i\}} l},$$

with i one particular direction ($i \in \{x_0, y_0, z_0\}$). To obtain a symmetric behavior, *i.e.* the same stiffness constant k_d whatever the shearing direction, it is possible to choose the average of the stiffness constants, with:

$$k_d = \frac{E\left(x_0^2 + y_0^2 + z_0^2\right)^2}{24\ (1+\nu)\ x_0\ y_0\ z_0}. \tag{8}$$

But, this solution may not be satisfying for all shearing experiments. However a unique solution can be obtained for a cubic element *i.e.* with $x_0 = y_0 = z_0$. In this case, k_d is well defined proportionally to G, with

$$k_d = \frac{3\ E\ x_0}{8\ (1+\nu)} = \frac{3}{4}\ G\ x_0. \tag{9}$$

Thus, after finding the expression of the stiffness constant k_d, we can continue our parameterization with the elongation experimentation to obtain the stiffness constants of the others edge springs.

Elongation experiment

As seen before, three equations result from each elongation experiment. Consequently, for each direction, the elongation experiment induces an over-constrained system with 3 equations and only one unknown. So, as in 2D, we will introduce two correction forces for each elongation direction.

Let apply a stress $F_{x_0}/(x_0 y_0)$ along the x_0 axis involving a stretching η along this axis. This stress also generates a thinning down on the orthogonal faces of 2ϵ along y_0 axis and of 2ζ along z_0 axis.

Thus, for this elongation experiment, the deformation of the diagonal springs is defined by:

$$\begin{aligned} d_d &= \sqrt{(x_0+\eta)^2 + (y_0 - 2\epsilon)^2 + (z_0 - 2\zeta)} - \sqrt{x_0^2 + y_0^2 + z_0^2} \\ &\sim \frac{\eta\ x_0 - 2\ \epsilon\ y_0 - 2\ \zeta\ z_0}{\sqrt{x_0^2 + y_0^2 + z_0^2}} + O(\eta^2, \epsilon^2, \zeta^2) \end{aligned}$$

Then, two Lagrange multipliers are linked to the forces induced by the spring distortions to ensure the correct integration of Poisson's ratio. Consequently, we have two new forces: $F_{x_{0_{y_0}}}$ and $F_{x_{0_{z_0}}}$ acting along y_0 and z_0, respectively. These corrective forces is generated for each one of the 8 vertices of the 3D element. Hence, the lagrangian associated to this elongation experiment along x_0, involving 4 springs of each direction (x_0, y_0, z_0) and 4 inner diagonals, is defined by:

$$\begin{aligned} L &= F_{x_0}\eta - 8F_{x_{0_{y_0}}}(2\epsilon) - 8F_{x_{0_{z_0}}}(2\zeta) - \frac{4}{2}k_{x_0}\eta^2 \\ &\quad -\frac{4}{2}k_{y_0}\left(2\epsilon\right)^2 - \frac{4}{2}k_{z_0}\left(2\zeta\right)^2 - \frac{4}{2}k_d\ d_d^2 \end{aligned}$$

Consequently, the energy minimization is calculated for

$$\frac{\partial L}{\eta} = 0, \frac{\partial L}{\epsilon} = 0, \frac{\partial L}{\zeta} = 0$$

and after resolution we obtain 3 equations (one deriving from Young's modulus and two from Poisson's ratio). Then, we iterate this process for

- an elongation experiment along y_0 induced by a force F_{y_0} with corrective forces $F_{y_{0_{x_0}}}$ along x_0 and $F_{y_{0_{z_0}}}$ along z_0,
- an elongation experiment along z_0 induced by a force F_{z_0} with corrective forces $F_{z_{0_{x_0}}}$ along x_0 and $F_{z_{0_{y_0}}}$ along y_0.

At the end, we obtain 9 equations with 9 unknown values and the system resolution gives us the following expected symmetric solutions, with $(i,j,k) \in \{x_0, y_0, z_0\}^3$ with $i \neq j \neq k$:

$$k_i = \frac{E\left(6\ j^2k^2\left(1+\nu\right) + \left(\nu(j^2+k^2) - i^2\right)\left(x_0^2 + y_0^2 + z_0^2\right)\right)}{24\ (1+\nu)\ x_0\ y_0\ z_0}$$

$$F_{i_j} = -\frac{\left(\left(x_0^2 + y_0^2 + z_0^2\right)\left(\nu(k^2+i^2) - i^2\right) + 6\ i^2\ k^2\ \nu\right)\ F_i}{48\ i\ j\ k^2} \tag{10}$$

Moreover, for a cubic element, *i.e.* with $x_0 = y_0 = z_0$, we obtain for $i \in \{x_0, y_0, z_0\}$:

$$k_{x_0} = \frac{E\ x_0\ (4\nu+1)}{8\,(1+\nu)},\ F_{\perp i} = -\frac{F_i(4\nu-1)}{16}. \tag{11}$$

To sum up, each element of our 3D mass-spring system is defined by 16 springs with four different stiffness constants (k_d, k_{x_0}, k_{y_0}, k_{z_0}) and by 6 corrective forces ($F_{x_{0_{y_0}}}, F_{x_{0_{z_0}}}, F_{y_{0_{x_0}}}, F_{y_{0_{z_0}}}, F_{z_{0_{x_0}}}, F_{z_{0_{y_0}}}$). These coefficients and corrective forces are defined by equations (8) and (10) which integrate Young's modulus and Poisson's ratio of the simulated deformable object. In the case of a cubic element, stiffness constants and corrective forces are defined by equations (9) and (11).

4.2.4 *Validation of the Bulk Modulus*

Before looking at the simulation loop, we want to validate our model according to its induced Bulk modulus.

In that sense, we apply a uniform pressure P on the surface of our 3D element. This pressure generate, for each couple of parallel faces, a force proportional to this pressure P: F_{Px_0} on plane (y_0, z_0), F_{Py_0} on plane (x_0, z_0) and F_{Pz_0} on plane (x_0, y_0). Thus, we have:

$$P = \frac{F_{Px_0}}{y_0\ z_0} = \frac{F_{Py_0}}{x_0\ z_0} = \frac{F_{Pz_0}}{x_0\ y_0}$$

$$\Rightarrow F_{Px_0} = P\ y_0\ z_0,\ F_{Py_0} = P\ x_0\ z_0,\ F_{Pz_0} = P\ x_0\ y_0.$$

These forces generate symmetrical deformations of 2η along x_0, 2ϵ along y_0, 2ζ along z_0 and a deformation of δ for the inner diagonals. Moreover, corrective forces due to each elongation are applied on each vertex of the 3D element. Thus, the Lagrangian equation of this compressibility experiment, involving all springs, is defined by:

$$\begin{aligned} L = {} & 2\eta\ P\ y_0\ z_0 + 2\epsilon\ P\ x_0\ z_0 + 2\zeta\ P\ x_0\ y_0 \\ & -8 \times 2\,\eta\,(F_{y_{0x_0}} + F_{z_{0x_0}}) - 8 \times 2\,\epsilon\,(F_{x_{0y_0}} + F_{z_{0y_0}}) \\ & -8 \times 2\,\zeta\,(F_{x_{0z_0}} + F_{y_{0z_0}}) - \tfrac{4}{2}k_{x_0}\,(2\eta)^2 \\ & -\tfrac{4}{2}k_{y_0}\,(2\epsilon)^2 - \tfrac{4}{2}k_{z_0}\,(2\zeta)^2 - \tfrac{4}{2}k_d\,\delta^2 \end{aligned}$$

The resolution of the energy minimization enables to obtain the expressions of the deformations η, ϵ and ζ. Then we can apply the Bulk modulus definition to introduce the compressibility equation as follow:

$$\Delta P = K\frac{\Delta V}{V_0} \Rightarrow K = \frac{\Delta P\ V_0}{\Delta V}$$

with V_0 (*resp.* P_0) the initial volume (*resp.* pressure), V_1 (*resp.* P_1) the volume (*resp.* pressure) after deformation and with $\Delta P = P_1 - P_0$, $\Delta V = V_1 - V_0$, $V_0 = x_0\ y_0\ z_0$ and $V_1 = (x_0 + 2\eta)\,(y_0 + 2\epsilon)\,(z_0 + 2\zeta)$.

Then, by assuming that $\Delta P \rightarrow 0$, we can find the definition of K, that is

$$K = \frac{E}{3\,(1 - 2\nu)}$$

and conclude that our 3D model enable the conservation of the Bulk modulus.

5 Simulating an Object Deformation

Since all the stiffness coefficients and the added corrective forces are now determined for a 2D or 3D mesh element, we can now present how we proceed to do the simulation of any object composed by these mesh elements.

5.1 Composition of elementary elements

Any deformable object can be modeled by the assembly of our 2D or 3D elements. Then, we apply on this later composition the several characteristics that just have been found in previous sections.

5.1.1 Mass-spring modeling of the composition

Fig. 6 presents a sample for a 2D object composed of 9 elementary 2D elements of our model. These 9 elements are placed side by side and consequently some springs appear twice in this composition.

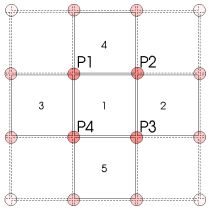

Fig. 6. A complex object is modeled by the assembly of several elementary "bricks" of our model.

For example in Fig. 6, vertices P_2 and P_3 are common to elements 1 and 2, and consequently, the spring between these two vertices appear twice. So, according to the parallel springs properties, we choose to model these two springs by a unique spring, linking vertices P_2 and P_3 with a stiffness constant equal to the sum of the stiffnesses of the two initial springs of elements 1 and 2.

From the energetic point of view of the simulated object, the total energy of an object corresponds to the sum of the energies of composing elements of this object. Thus, the Lagrangian equation describing the behavior of the object corresponds to the superposition of the Lagrangian equation of each element. Moreover, external forces applied to an element of the object, follows (i) from forces due to the neighboring elements, and (ii) from external forces of the object.

5.1.2 Tensile properties of the composition

Then, we want to validate this composition by demonstrating that the tensile properties (Young's modulus and Poisson's ratio) are preserved. For this, let consider a bar of size $l_0 \times h_0$ composed of n elements i. Moreover, we assume that these elements, of sizes $l_0 \times h_i$ with $\sum_{i=1}^{n} h_i = h_0$, have the same Young's modulus and Poisson's ratio.

First, we assume that the bar is fixed at its base of size l_0, and we apply at its extremity a tensile force F_{h_0} according to the direction h_0. When the bar is at its equilibrium, the sum of the internal forces of each element are null. Moreover, as the bar is a composition of several elements in equilibrium, the tensile force applied at the extremity of the bar, induced the application of this force on each element composing this bar. Consequently, each element find its equilibrium for a same stress F_{h_0}/l_0.

We note η_i and $2\delta_i$ the strains caused by F_{h_0} on each element i of size $h_i \times l_0$. Then, as each element has the

same Young's modulus and Poisson's ratio, we have:

$$E = \frac{F_{h_0}/l_0}{\eta_i/h_i}, \;\; \nu = \frac{2\delta_i/l_0}{\eta_i/h_i}.$$

$$\Rightarrow \eta_i = \frac{h_i \; F_{h_0}}{E \; l_0}, \;\; \delta_i = \nu \; l_0 \frac{\eta_i}{2h_i} = \frac{\nu \; F_{h_0}}{2 \; E}.$$

Thus, we can note that the expression of η_i is independent of the element. So, if we consider the bar as a unique element of size $l_0 \times h_0$, we have:

$$\eta = \sum_{i=1}^{n} \eta_i = \frac{F_{h_0}}{E \; l_0} \sum_{i=1}^{n} h_i = \frac{F_{h_0} \; h_0}{E \; l_0},$$

$$\delta = \delta_i = \frac{\nu \; F_{h_0}}{2 \; E}.$$

So, using the Young's modulus and Poisson's ratio definitions on the bar, we obtain:

$$E_{bar} = \frac{F_{h_0}/l_0}{\eta/h_0} = \frac{F_{h_0}/l_0}{F_{h_0}/E \; l_0} = E,$$

$$\nu_{bar} = \frac{2\delta/l_0}{\eta/h_0} = \frac{2\delta}{l_0} \times \frac{h_0}{\eta} = \frac{2\nu F_{h_0}/2E}{l_0} \times \frac{h_0}{F_{h_0}/E \; l_0} = \nu$$

Consequently, the conservation of the Young's modulus and Poisson's ratio of the bar is validated for the tensile test according to the direction of the assembly.

Then, we have to do the same tensile test, but with a traction orthogonal to the assembly. So, we assume now that the bar is fixed at a orthogonal side to the base, and we apply a pressure P_{l_0} on the other orthogonal side along to the direction l_0.

Thus, we apply on each element i a force $F_{l_0,i}$ with $F_{l_0,i} = h_i \; P_{l_0}$ and we note ${\eta'}_i$ and $2{\delta'}_i$ the resulting strains. Consequently, as each element has the same Young's modulus and Poisson's ratio, we have:

$$E = \frac{F_{l_0,i}/h_i}{{\eta'}_i/l_0}, \;\; \nu = \frac{2{\delta'}_i/h_i}{{\eta'}_i/l_0},$$

$$\Rightarrow {\eta'}_i = \frac{F_{l_0,i} \; l_0}{E \; h_i} = \frac{l_0 \; P_{l_0}}{E}, \;\; {\delta'}_i = \frac{\nu \; h_i \; {\eta'}_i}{2 \; l_0} = \frac{\nu \; h_i \; P_{l_0}}{2 \; E}.$$

Thus, we can note that the deformation ${\eta'}_i$ is a constant. Moreover, if we consider again the bar as a unique element of size $l_0 \times h_0$, we have:

$$\eta' = {\eta'}_i, \;\; \delta' = \sum_{i=1}^{n} {\delta'}_i = \frac{\nu \; P_{l_0}}{2 \; E} \sum_{i=1}^{n} h_i = \frac{\nu \; P_{l_0} \; h_0}{2 \; E}$$

So, using the Young's modulus and Poisson's ratio definitions on the bar, we obtain:

$$E_{bar} = \frac{P_{l_0}}{\eta'/l_0} = P_{l_0} \times \frac{l_0}{\eta'} = \frac{P_{l_0} \; l_0 \; E}{l_0 \; P_{l_0}} = E,$$

$$\nu_{bar} = \frac{2\delta'/h_0}{\eta'/l_0} = \frac{2\delta'}{h_0} \times \frac{l_0}{\eta'} = \frac{2 \; \nu \; P_{l_0} \; h_0}{2E \; h_0} \times \frac{l_0 \; E}{l_0 \; P_{l_0}} = \nu.$$

Consequently, we also obtain the conservation of the Young's modulus and Poisson's ratio for a tensile test orthogonal to the assembly.

Moreover, note that the same results are obtained for the shear modulus and for tests with a bar of $n \times m$ elements. So, the assembly exhibits the same mechanical characteristics as each element composing it, and this independently of the size of the element.

5.2 Simulation Loop

We have seen that a deformable objet is modeled by the assembly of several 2D or 3D elements of our MS model. Then, the simulation of this object results from the simulation of the deformation of each single element that constitutes the object.

This simulation can be done according to Newton's laws. In this case, the several steps of the simulation loop are as follows:

1) Computation of all forces applied to each element. These forces can be (i) internal, including forces due to springs and correction forces, or (ii) external, like gravity or reaction forces due to neighborhood.
2) Computation of accelerations of each element according to Newton's laws.
3) Computation of velocities and positions of each element according to any numerical integration scheme.

After the description of our 2D or 3D model, we will present in the next section some numerical experimentations.

6 Evaluation of the 3D Model

We propose now to qualify the mechanical properties of our system. For this, we have carried out several tests.

6.1 Tensile stress experiment

We start our experimentations with some tensile stress tests by applying to a beam-like object a quasi-static stress. The elongation can attain 20% of the beam length. The experiments have been carried out with input parameters ranging from 100 Pa to 100 kPa for Young's modulus E, and from 0.1 to 0.5 for Poisson's ratio ν. The accuracy of the simulation is evaluated by comparing the simulated mechanical quantities to the input parameters.

The quantitative study of the test results shows that Young's modulus (see Fig. 7) and Poisson's ratio (see Fig. 8) of our model tend to drift when the deformation increases. Nevertheless, these results are really satisfying. As illustrated in Fig. 7, the error on Young's modulus exceeds 5% only for deformations larger than 10%. Besides, we notice that this error increases conversely with the imposed Poisson's ratio: for a 10% deformation, the error on Young's modulus amounts to 2.7% if $\nu = 0.3$ and it amounts only to 2% if $\nu = 0.4$. This error falls down to 1.5% when $\nu = 0.5$.

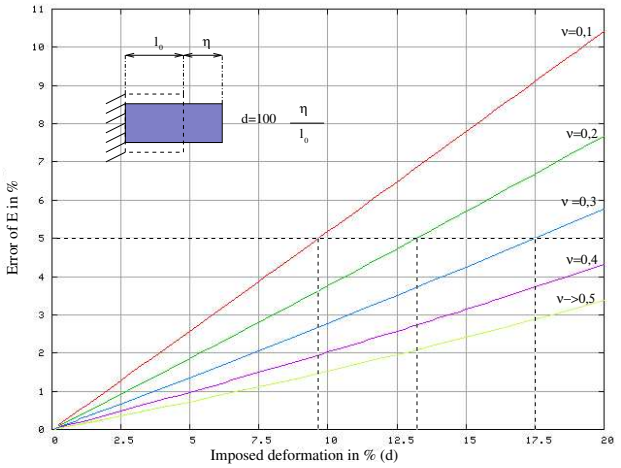

Fig. 7. Errors on Young's modulus for a cubic meshed element in quasi-static tensile stress.

The Fig. 8 illustrates that, concerning Poisson's ratio simulation, the error for $\nu \in [0.3; 0.5]$ remains lower than 5%, even if the deformation attains 14%. We observe identical curves whatever the value of E is. This is not surprising since the spring stiffness constants and the thinning forces are proportional to the input parameter E. We point out a change in the profile of Poisson's ratio error occurring at $\nu = 0.25$. Thinning is overestimated for values of $\nu \geq 0.25$ and underestimated elsewhere. In fact, at $\nu = 0.25$, no corrective Lagrangian forces are needed, so the error is minimal.

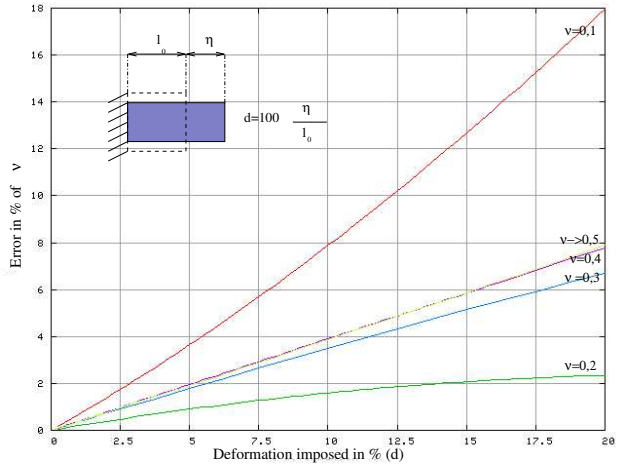

Fig. 8. Poisson's ratio errors (absolute value) for a cubic element in tensile stress.

When performing tensile tests on a beam, meshed by any composition of elements, we obtain exactly the same error as for a unique element. This confirms that the mechanical properties of any meshed object are fully defined by the properties of the mesh elements.

6.2 Shearing experiment

Then, we continue our experimentations with some shearing experiments. To validate the shearing on an element composition, we built a $100\times100\times300$ mm beam by assembling elements characterized by $E = 1$ Pa and $\nu = 0.3$. We stressed it by applying a force equivalent to 2000 N. The interpretations of shearing experiment are not straightforward for large deformations. Therefore, we considered as reference the FEM solution to evaluate the accuracy of our model. For this, results of our simulations have been superimposed to the FEM one (see Fig. 9). Within the framework of our model, *i.e.* small deformations, the agreement is very satisfactory, attesting the good behavior of our model.

Fig. 9 illustrates the influence of the mesh resolution on the result accuracy. We observe a mean error in displacement around 13% with a maximum of 33% for a $2\times2\times6$ resolution. It decreases progressively when we improve the resolution. Mean and maximal errors fall down respectively to 3% and 6% for a $8\times8\times24$ resolution. We performed additional experiments that show convergence of our method when refining mesh, that what one of the major drawback of most early techniques.

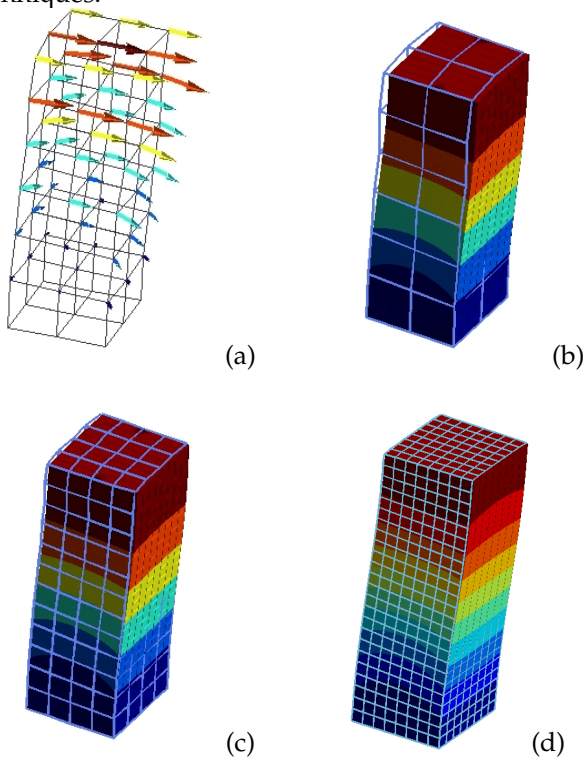

(a-b) $2\times2\times6$ sampling: M=13%, SD=1.3% MAX=33%
(c) $4\times4\times12$ sampling: M=6%, SD=0.33% MAX=14%
(d) $8\times8\times24$ sampling: M=3%, SD=0.03% MAX=6%

Fig. 9. Shearing experience: (a) Map of error in displacement on each node of the mesh, (b-d) the reference FEM solution (in color gradation) with superimposition of various simulations performed for different sampling resolutions (wire mesh). *Notation: M for mean error value, SD for standard deviation and MAX for maximal error.*

On Fig. 10, we can also remark that the relative error on G does not depend on E, as expected. This error increases with the imposed ν but remains smaller than 5% for a shearing angle inferior to $5°$ and for $\nu < 0.4$.

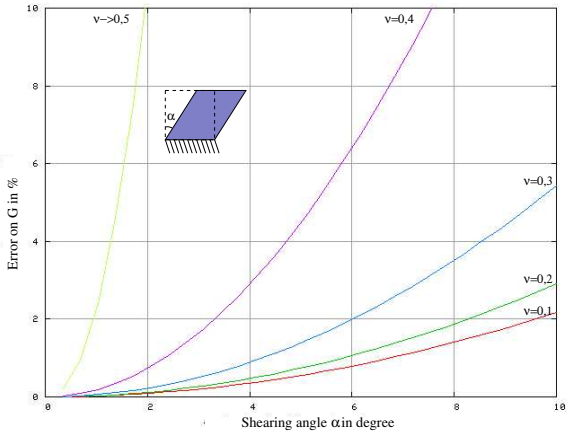

Fig. 10. G errors for a cubic element according to an imposed shearing deformation and the Poisson's ratio.

Then, we realize this shearing experiment on a non-symmetric composition. For this, we choose an L-shaped object fixed at its base, and we apply a constant force to the edges orthogonal to the base. Fig. 11 shows our results superimposed to the FEM solution (computed at high resolution), with a map of deformation. The object dimensions are 4000×4000×4000mm. The mechanical characteristics are: Young's modulus of 1kPa, Poisson's ratio of 0.3 and an applied force of 0.3GN. In this experiment, we have neglected the mass.

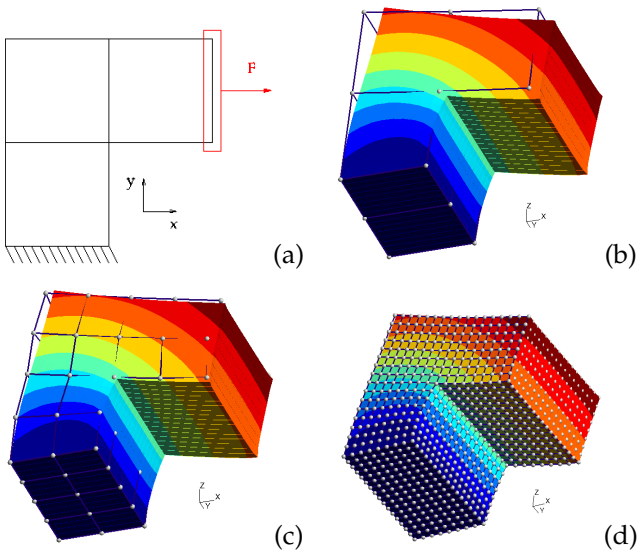

(b) 2×2×2: M=6.99%, SD=0.94%, MAX=18%.
(c) 4×4×4: M=3.37%, SD=0.20%, MAX=7%.
(d) 8×8×8: M=0.66%, SD=0.01%, MAX=1.6%.

Fig. 11. Experiment on a non-symmetric object: (a) load scheme, (b-d) the reference FEM solution (in color gradation) with superimposition of various simulations performed for different sampling resolutions (wire mesh).

Again we clearly observe that our model behaves as expected *i. e.* better mesh resolution leads to better results. Moreover, the dissymmetry of the geometry does not influence the accuracy of the results.

6.3 Deflection experiment

Then, we continue our experimentations. Indeed, the deflection experience (construction or structural element bends under a load) is recommended to validate mechanical models. It constitutes a relevant test to evaluate (a) the mass repartition, and (b) the behavior in case of large deformations inducing large rotations, especially close to the fixation area.

This test consists in observing the deformation of a beam anchored at one end to a support. At equilibrium, under gravity loads, the top of the beam is under tension while the bottom is under compression, leaving the middle line of the beam relatively stress-free. The length of the zero stress line remains unchanged (see Fig. 12).

In case of a null Poisson's ratio, the load induced deviation of the neutral axis is given by:

$$y\,(x) = \frac{\rho g}{24\ EI}\left(6\ L^2x^2 - 4\ L\ x^3 + x^4\right) \qquad (12)$$

for a parallelepiped beam of inertia moment $I = TH^3/12$, and with linear density $\rho = M/L$.

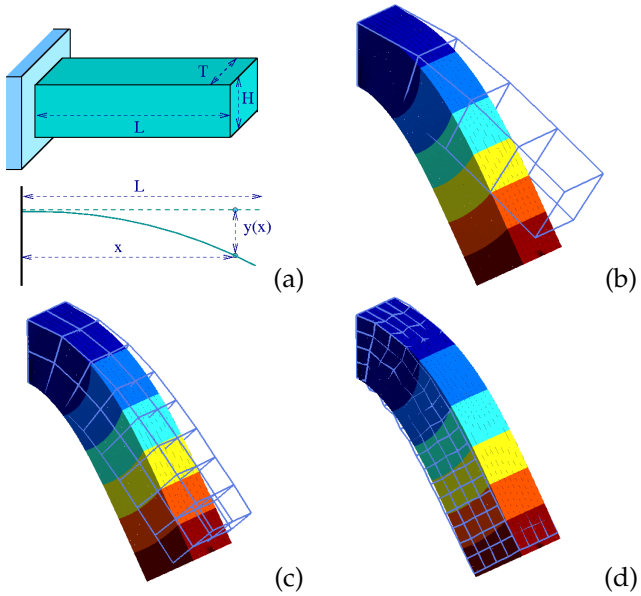

(b) 4×1×1: M=16.31%, SD=2.83%, MAX=38%.
(c) 8×2×2: M=7.08%, SD=0.58%, MAX=16.7%.
(d) 16×4×4: M=0.68%, SD=0.03%, MAX=4.05%.

Fig. 12. Deflection experiment: (a) Cantilever neutral axis deviation, (b-d) the reference FEM solution (in color gradation) with superimposition of various simulations performed for different sampling resolutions (wire mesh).

We notice that results are dependent of the sampling resolution, as for any other numerical method, however the fiber axis profile remains close to the profile given by equation (12). Fig. 12 displays some results for a

cantilever beam of dimensions $400\times100\times100$ mm, with Young's modulus equals to 1000 Pa, Poisson's ratio to 0.3 and a mass of 0.0125 Kg.m^{-3}. By looking at the displacement errors at each mesh node, we observe that the error is decreasing when the sampling is improved: the maximum error in the sampling $4 \times 1 \times 1$ is about 45% while it is about 5% for a resolution of $16 \times 4 \times 4$, compared to a FEM reference result (computed at higher resolution), proving again the convergent behavior of our technique.

6.4 3D deformable object simulation

An example of application is depicted on Fig. 13.

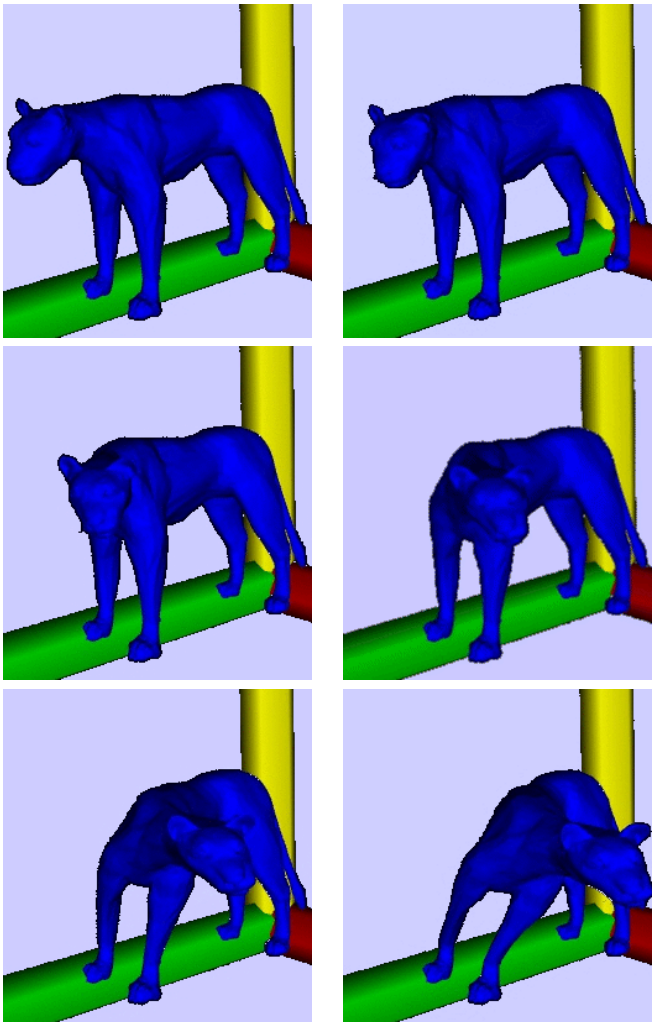

Fig. 13. A complete 3D application: simulation of the head lateral movement at different steps. *Puma's model developed by the INRIA Gamma researcher's team.*

By dragging points, we applied some external forces on an initial hexahedral meshing of a puma, leading to produce the head lateral movement. Note that the initial choice of a parallelepiped shape is absolutely not a constraint in most applications. This choice has been motivated by the fact that it is considered by the numerical community as stable and more precise for the same number of elements than a tetrahedral mesh element. This is to be counterbalanced by the fact that it requires generally more elements to fit a non simple geometry. Anyway, for better visualization or collision detection purposes, it is easy to fit a triangular skin on our hexahedral model, as shown on Fig. 13.

7 Conclusion and Future Work

We proposed a mass-spring model that ensures fast and physically accurate simulation of linear elastic, isotropic and homogeneous material. It consists in meshing any object by a set of cubic mass-spring elements. By construction, our model is well characterized by the Young's modulus and Poisson's ratio. The spring coefficients have just to be initialized according to simple analytic expressions. The precision of our model have been given, by comparing our results with those obtained by a high resolution finite element method, chosen as reference.

In the future, we are looking to apply the same techniques to other geometrical elements, for example tetrahedron or any polyhedron. This would increase the geometrical reconstruction possibilities and would offer more tools for simulating complex shapes, although in the actual state, the hexahedral shape is not a constraint in many applications ranging from mechanics to medicine. If desired, a triangulation of the surface can be performed with ease and at reduced computational cost.

Mesh optimization or local mesh adaptation would probably improve the efficiency of the model. For example, we can modify the resolution in the vicinity of highly deformed zones, reducing large rotations of elements undergoing heavy load.

We exhibited that our model can support reasonably large deformations. The accuracy increases with the mesh resolution. This is a major improvement relatively to early techniques, as it is generally dependent to the mesh resolution and topology. However, it may be interesting to investigate a procedure to update the spring coefficients and corrective forces when the deformations become too large. In this case, the elastic behaviour will be lost (the initial shape will not be recovered), but this may allow to handle strong topology alteration, even melting should be able to be considered.

REFERENCES

[1] Vincent Baudet. *Modélisation et simulation paramétrable d'objets déformables*. PhD thesis, Université Lyon 1, 2006.

[2] Gérald Bianchi, Barbara Solenthaler, Gàbor Székely, and Matthias Harders. Simultaneous topology and stiffness identification for mass-spring models based on FEM reference deformations. In Springer-Verlag, editor, *MICCAI 2004*, pages 293–301, Berlin, 2004.

[3] David Bourguignon. *Interactive Animation and Modeling by Drawing - Pedagogical Applications in Medicine*. PhD thesis, Institut National Polytechnique de Grenoble, 2003.

[4] François Boux de Casson. *Simulation dynamique de corps biologiques et changements de topologie interactifs*. PhD thesis, Université de Savoie, 2000.

[5] Cynthia Bruyns and Mark Ottensmeyer. Measurements of soft-tissue mechanical properties to support development of a physically based virtual anima model. In *MICCAI 2002*, pages 282–289, 2002.

[6] Stéphane Cotin, Hervé Delingette, and Nicholas Ayache. Efficient linear elastic models of soft tissues for real-time surgery simulation. *Proceedings of the Medecine Meets Virtual Reality (MMVR 7)*, 62:100–101, 1999.

[7] Gilles Debunne. *Animation multirésolution d'objets déformables en temps réel, Application la simulation chirurgicale*. PhD thesis, Institut National Polytechnique de Grenoble, 2000.

[8] Herve Delingette. Triangular springs for modeling nonlinear membranes. *IEEE Transactions on Visualization and Computer Graphics*, 14(2):329–341, 2008.

[9] O. Deussen, L. Kobbelt, and P. Tucke. Using simulated annealing to obtain good nodal approximations of deformable objects. In Springer-Verlag, editor, *Proceedings of the Sixth Eurographics Workshop on Animation and Simulation*, pages 30–43, Berlin, 1995.

[10] R. Feynman. *The Feynman Lectures on Physics*, volume 2. Addison Wesley, 1964. chapter 38.

[11] Michael Keckeisen, Olaf Etzmuß, and Michael Hauth. Physical models and numerical solvers for cloth animations. In *Simulation of Clothes for Real-time Applications*, volume Tutorial 1, pages 17–34. INRIA and the Eurographics Association, 2004.

[12] B.A. Lloyd, G. Szkely, and M. Harders. Identification of spring parameters for deformable object simulation. *IEEE Trans. on Visualization and Computer Graphics*, 13(5):1081–1094, Sept-Oct 2007.

[13] Jean Louchet, Xavier Provot, and David Crochemore. Evolutionary identification of cloth animation models. In Springer-Verlag, editor, *Proceedings of the Sixth Eurographics Workshop on Animation and Simulation*, pages 44–54, Berlin, 1995.

[14] A. Luciani, S. Jimenez, J. L. Florens, C. Cadoz, and O. Raoult. Computational physics: A modeler-simulator for animated physical objects. In *Proceedings of Eurographics 91*, pages 425,436, Amsterdam, 1991. Eurographics.

[15] Anderson Maciel, Ronan Boulic, and Daniel Thalmann. *Deformable Tissue Parameterized by Properties of Real Biological Tissue*, volume 2673 of *Lecture Notes in CS: Surgery Simulation and Soft Tissue Modeling*, pages 74–87. Springer, 2003.

[16] U. Meier, O López, C. Monserrat, M. C. Juan, and M. Alcañiz. Real-time deformable models for surgery simulation : a survey. *Computer Methods and Programs in Biomedicine*, 77(3):183–197, 2005.

[17] Philippe Meseure and Christophe Chaillou. Deformable body simulation with adaptative subdivision and cuttings. In *5th Int. Conf. in Central Europe on Comp. Graphics and Visualisation WSCG'97*, pages 361–370, 1997.

[18] A. Nealen, M. Mller, R. Keiser, E. Boxerman, and M. Carlson. Physically based deformable models in computer graphics. *Computer Graphics Forum*, 25(4):809–836(28), December 2006.

[19] Luciana Porcher Nedel and Daniel Thalmann. Real-time muscles deformations using mass-spring systems. *Computer Graphics International*, pages 156–165, 1998.

[20] Céline Paloc. *Adaptative Deformable Model (allowing Topological Modifications) for Surgical Simulation*. PhD thesis, University of London, 2003.

[21] Guillaume Picinbono, Hervé Delingette, and Nicholas Ayache. Non-linear anisotropic elasticity for real-time surgery simulation. *Graphical Model*, 2003.

[22] Emmanuel Promayon, Pierre Baconnier, and Claude Puech. Physically based deformation constrained in displacements and volume. In *Proceedings of Eurographics'96*, Oxford, 1996. BlackWell Publishers.

[23] Xavier Provot. Deformation constraints in a mass-spring model to describe rigid cloth behavior. In *Proceedings of Graphics Interface 95*, pages 147,154, Toronto, 1995. Canadian Human-Computer Communications Society.

[24] D. Terzopoulos and K. Waters. Physically-based facial modelling, analysis, and animation. *The Journal of Visualization and Computer Animation*, 1:73–80, 1990.

[25] Allen Van Gelder. Approximate simulation of elastic membranes by triangulated spring meshes. *Journal of Graphics Tools*, 3(2):21–42, 1998.

[26] Jane Wilhelms and Allen Van Gelder. Anatomically based modelling. In *Computer Graphics (SIGGRAPH'97 Proceedings)*, pages 173–180, 1997.